mathematics

MDPI

Article

Hybrid Backstepping Control of a Quadrotor Using a Radial Basis Function Neural Network

Muhammad Maaruf [1], Waleed M. Hamanah [2,3] and Mohammad A. Abido [2,4,5,*]

[1] Control and Instrumentation Engineering Department, Center for Smart Mobility and Logistics, King Fahd University of Petroleum and Minerals, Dhahran 31261, Saudi Arabia
[2] Interdisciplinary Research Center of Renewable Energy and Power Systems (IRC-REPS), King Fahd University of Petroleum and Minerals, Dhahran 31261, Saudi Arabia
[3] Applied Research Center for Metrology, Standards and Testing (ARC-MST), King Fahd University of Petroleum and Minerals, Dhahran 31261, Saudi Arabia
[4] Department of Electrical Engineering, College of Engineering and Physics, King Fahd University of Petroleum and Minerals, Dhahran 31261, Saudi Arabia
[5] K.A.CARE Energy Research & Innovation Center, King Fahd University of Petroleum and Minerals, Dhahran 31261, Saudi Arabia
* Correspondence: mabido@kfupm.edu.sa

Abstract: This article presents a hybrid backstepping consisting of two robust controllers utilizing the approximation property of a radial basis function neural network (RBFNN) for a quadrotor with time-varying uncertainties. The quadrotor dynamic system is decoupled into two subsystems: the position and the attitude subsystems. As part of the position subsystem, adaptive RBFNN backstepping control (ANNBC) is developed to eliminate the effects of uncertainties, trace the quadrotor's position, and provide the desired roll and pitch angles commands for the attitude subsystem. Then, adaptive RBFNN backstepping is integrated with integral fast terminal sliding mode control (ANNBIFTSMC) to track the required Euler angles and improve robustness against external disturbances. The proposed technique is advantageous because the quadrotor states trace the reference states in a short period of time without requiring knowledge of dynamic uncertainties and external disturbances. In addition, because the controller gains are based on the desired trajectories, adaptive algorithms are used to update them online. The stability of a closed loop system is proved by Lyapunov theory. Numerical simulations show acceptable attitude and position tracking performances.

Keywords: quadrotor; radial basis function neural network; backstepping; adaptive control; integral fast terminal sliding mode control

MSC: 93-10

Citation: Maaruf, M.; Hamanah, W.M.; Abido, M.A. Hybrid Backstepping Control of a Quadrotor Using a Radial Basis Function Neural Network. *Mathematics* **2023**, *11*, 991. https://doi.org/10.3390/math11040991

Academic Editors: Krzysztof Ejsmont, Aamer Bilal Asghar, Yong Wang and Rodolfo Haber

Received: 4 January 2023
Revised: 6 February 2023
Accepted: 8 February 2023
Published: 15 February 2023

1. Introduction

Quadrotors have a simple mechanical structure and lighter weight, which enable them to perform aggressive operation, hovering, vertical take-up, and landing [1,2]. Many remarkable applications are accomplished using quadrotor platforms, such as aerial cinematography, mapping, payload delivery, and rescue mission surveillance, to name just a few [3–5]. A control system architecture for achieving the practical application of quadrotors is one of the key problems that must be discussed. Without a strong control system, the quadrotors would be seriously limited in operation. Therefore, several studies on the design of the quadrotor control system have been carried out.

In the early stages of quadrotor control research, linear control techniques such as linear quadratic regulator (LQR) and proportional derivative integral (PID) control [6–11] were adopted. Both PID and LQR are linear control strategies and were used to stabilize the quadrotor attitude and position by linearizing the dynamics of the quadrotor near some operating points. As a result, the performances of the quadrotor, such as the robustness

against dynamic uncertainties and environmental disturbances and trajectory tracking accuracy, were poor [12]. With the advancement of control methods and the wide applications of quadrotors, several nonlinear control technologies have been developed and have accomplished effective performances.

One of the popular nonlinear control strategies is backstepping control, which has been widely applied to nonlinear systems in recent years. This technique guarantees the asymptotic stability of nonlinear systems through a recursive design procedure. A backstepping control method was applied to the Lagrangian model of a quadrotor [13]. In [14], backstepping and proportional derivative (PD) controllers were used for the quadrotor attitude and position control, respectively. In [**?**], a flight controller was designed based on a fractional-order backstepping control. The downside of a backstepping controller is that it requires an accurate model of the system. In order to account for the uncertain parameters, an adaptive backstepping controller has been implemented for a quadrotor with varying parameters [16–18]. In [19], an adaptive finite time backstepping controller was designed for a quadcopter UAV.

Another popular nonlinear control technique applied to the quadrotors is sliding mode control. A sliding mode control is a robust control scheme that counters uncertainties and disturbances [20–22] in dynamic systems. In a conventional sliding control strategy, it is assumed that the upper bounds of the disturbances are known. Unlike backstepping control, sliding mode control has a simple structure and is easier to implement. In [23], an integral sliding mode controller was proposed to control a quadrotor with uncertainties and external disturbances. In [24], a sliding mode attitude controller was proposed for a quadrotor with time-varying mass. In [25], a second-order sliding mode control of an uncertain quadrotor was investigated. A sliding mode control with exponential reaching law and disturbance compensator was successfully applied to a quadrotor [26]. A robust fast terminal sliding mode controller was developed for a quadrotor [27–29]. A nonsingular terminal sliding mode controller was proposed in [30] for orientation and position tracking of a quadrotor with rotor failure. In [31], a trajectory tracking control of a quadrotor was achieved with a sliding mode controller and a robust integral of the signum error controller. Chattering-reduction sliding mode control of quadrotor was studied [32]. For a better suppression of disturbances, adaptive algorithms were used to estimate and compensate the upper-bounds of the disturbances. An adaptive fault tolerant controller was suggested for attitude control of a quadrotor [33]. An adaptive sliding mode controller was devised for the differential flat quadrotor model [34]. A finite time adaptive integral sliding mode controller was presented for an uncertain quadrotor [35]. In [36], an adaptive sliding mode controller was developed to counter external disturbances and and enhance the altitude tracking of the quadrotor. Recently, combinations of backstepping and sliding mode control approaches have gained attention. Robust trajectory control of a quadrotor was studied using a chattering free backstepping sliding mode controller [37]. A robust backstepping sliding mode controller was presented in [38] to accomplish a trajectory tracking control of a quadrotor. An adaptive backstepping fast terminal sliding mode controller was proposed for robust position and the attitude tracking of a quadrotor [39].

Another way of estimating disturbances in dynamic systems is by employing disturbance observers. In [40], a nonlinear disturbance observer-based control was proposed for a quadrotor to accurately land on a moving target. In [41], a high-gain observer-based controller was suggested for quadrotor control. In [42], a fixed time disturbance observer-based attitude controller was studied for aggressive maneuvering and disturbance rejection. In [43], a sliding mode observer was utilized for obstacle avoidance and robust trajectory tracking of a quadrotor. A backstepping sliding mode control with actuator fault observer was presented in [44]. A robust backstepping controller combined with extended state observer was used to tackle the trajectory tracking problem of a quadrotor in [45]. In [46], a disturbance observer-based altitude controller was used to facilitate accurate landing of a quadrotor on a vertically moving apron. In [47–49] an active disturbance rejection

control strategy was employed for trajectory tracking of quadrotor irrespective of the external disturbances.

Over the years, RBFNN and fuzzy logic systems have been widely used as function approximators in control system design [50]. A Fuzzy-Padé approximation controller was presented for the attitude tracking of a quadrotor [51]. In [52], a fuzzy approximator was used together with sliding mode control to compensate for faults. In [53], a robust fuzzy integral backstepping trajectory tracking controller was implemented for a quadrotor with input constraints. In [54–56], an adaptive RBFNN sliding mode control was suggested for attitude and position tracking of a quadrotor. In [57], attitude and position tracking controllers using RBFNN were applied to a coaxial octorotor. In [58], an adaptive robust controller with neural-disturbance estimator was proposed for a quadrotor to track a moving object. A neural backstepping controller was devised for a quadrotor to land on ship deck [59].

To stay current with the rapid advancements in technology, quadrotor control strategies must continue to develop in order to fulfill the demanding safety standards. To further improve the tracking performance of the quadrotor in various applications, the authors in [23] proposed a hierarchical control structure consisting of integral sliding mode control (ISMC) and backstepping sliding mode control (BSMC) to stabilize the position and attitude, respectively, of the quadrotor in the presence of disturbances. In [31], proportional-derivative sliding mode control (PD-SMC) and robust integral of the signum error control (RISE) were designed for the position and attitude of the quadrotor, respectively. However, in [23,31], the authors assumed that the disturbances are bounded by known positive terms. This assumption is too strict, because, in practical applications, the disturbances due to wind gusts and dynamic uncertainties are time-varying, and their upper bounds cannot be obtained accurately. Moreover, refs. [23,31] used discontinuous reaching laws that introduce chattering. Therefore, designing a new hierarchical control architecture that tackles the aforesaid issues while considering less computational complexities is an interesting problem to investigate.

Motivated by the aforesaid discussion, this work presents a new robust hybrid backstepping control scheme for a quadrotor under model uncertainties and disturbances. The quadrotor is partitioned into an inner loop and an outer loop. An ANNBC is designed for the outer loop position control. For the inner loop, an ANNBIFTSMC is designed for attitude control. The hybrid control structure, ANNBC-ANNBIFTSMC, has characteristics such as low computational burden, robustness against disturbances, fast convergence, and high tracking precision compared to some control techniques. The main contributions of this article are summarized as follows:

1. Unlike the ISMC [23] and PD-SMC [31] that were utilized to control the position of the quadrotor, this paper paper proposes an ANNBC to control the position of the quadrotor and generate the desired roll and pitch angles. The derivatives of the virtual controllers along with lumped time-varying disturbances are approximated with a single RBFNN to lessen the computation cost. Moreover, contrary to [23,31] where the controller gains are fixed, here, the controller gains are adjusted online in order to improve the tracking accuracy.
2. In contrast to BSMC and RISE, respectively, designed in [23,31] to control the attitude of the quadrotor, this work develops an ANNBIFTSMC strategy for the attitude subsystem to attain quick and smooth tracking of the desired angles despite the time-varying disturbances. A single RBFNN is utilized to approximate the uncertain nonlinear functions along with the disturbances and the gains of the IFTSM surfaces. This significantly reduces the computational burden. In addition, fast terminal reaching laws are employed to solve the chattering problems, unlike in [23,31]. Moreover, the gains of the chattering laws are updated online in order to properly adjust the convergence speed.
3. The superiority of the new ANNBC-ANNBIFTSMC is illustrated by comparing its performance with the results reported in [23,31].

This paper is arranged as follows. The under-actuated dynamic model of the quadrotor is presented in Section 2. The proposed ANNBC-ANNBIFTSMC is presented in Section 3. In addition, simulation results are presented in Section 4. The summary of the paper is provided in Section 5.

2. Mathematical Modelling

The nonlinear dynamic model of the quadrotor in state space is obtained as [35,39]:

$$\begin{cases} \dot{x}_1 = x_2 \\ \dot{x}_2 = \mathrm{a}_2 x_4 x_6 + \mathrm{a}_2 x_4 + \mathrm{a}_3 x_2^2 + \mathrm{g}_1 T_2 + \delta_{x_1} \\ \dot{x}_3 = x_4 \\ \dot{x}_4 = \mathrm{a}_5 x_2 x_6 + \mathrm{a}_5 x_2 + \mathrm{a}_6 x_4^2 + \mathrm{g}_2 T_3 + \delta_{x_3} \\ \dot{x}_5 = x_6 \\ \dot{x}_6 = \mathrm{a}_7 x_2 x_4 + \mathrm{a}_8 x_6^2 + \mathrm{g}_3 T_4 + \delta_{x_5} \\ \dot{x}_7 = x_8 \\ \dot{x}_8 = \mathrm{a}_9 x_8 + (C_{x_2} C_{x_5} S_{x_3} + S_{x_2} S_{x_5}) \frac{T_1}{m} + \delta_{x_7} \\ \dot{x}_9 = x_{10} \\ \dot{x}_9 = \mathrm{a}_{10} x_{10} + (C_{x_2} S_{x_3} S_{x_5} + C_{x_5} S_{x_2}) \frac{T_1}{m} + \delta_{x_9} \\ \dot{x}_{11} = x_{12} \\ \dot{x}_{12} = \mathrm{a}_{11} x_{12} - g + (C_{x_2} C_{x_3}) \frac{T_1}{m} + \delta_{x_{11}} \end{cases} \tag{1}$$

where x_1, x_3, x_5 stand for the roll, pitch, and yaw angles of the quadrotor, respectively, $x_2 = \dot{x}_1$, $x_4 = \dot{x}_3$, and $x_6 = \dot{x}_5$ denote the angular velocities of the quadrotor, x_7, x_9, and x_{11} represent the positions of the quadrotor in the inertia frame, $x_8 = \dot{x}_7$, $x_{10} = \dot{x}_9$, and $x_{12} = \dot{x}_{11}$ denote the linear velocities of the quadrotor, $C_{(.)}$ and $S_{(.)}$ stand for $cos(.)$ and $sin(.)$, respectively, $\mathrm{a}_1 = \frac{I_{yy} - I_{zz}}{I_x}$, $\mathrm{a}_2 = \frac{\Omega_r J_r}{I_x}$, $\mathrm{a}_3 = \frac{-K_{ax}}{I_{xx}}$, $\mathrm{a}_4 = \frac{I_{zz} - I_{xx}}{I_{yy}}$, $\mathrm{a}_5 = \frac{\Omega_r J_r}{I_{yy}}$, $\mathrm{a}_6 = \frac{-K_{ay}}{I_{yy}}$, $\mathrm{a}_7 = \frac{I_{xx} - I_{yy}}{I_{zz}}$, $\mathrm{a}_8 = \frac{-K_{az}}{I_{zz}}$, $\mathrm{a}_9 = \frac{-K_{dx}}{m}$, $\mathrm{a}_{10} = \frac{-K_{dy}}{m}$, $\mathrm{a}_{11} = \frac{-K_{dz}}{m}$, $\mathrm{g}_1 = \frac{L}{I_x}$, $\mathrm{g}_2 = \frac{L}{I_y}$, $\mathrm{g}_3 = \frac{L}{I_z}$, g is the acceleration due to gravity, I_x, I_y, I_z denote the inertias, m indicates the total mass of the quadrotor, K_{ax}, K_{ay}, K_{az}, $K_{a\phi}$, $K_{a\theta}$, and $K_{a\psi}$ stand for the the drag coefficients, $\Omega_r = (\Omega_1 - \Omega_2 + \Omega_3 - \Omega_4)$ is the relative speed of the quadrotor, Ω_i, $(i = 1, 2, 3, 4)$ are the rotor speeds related by

$$\begin{bmatrix} T_1 \\ T_2 \\ T_3 \\ T_4 \end{bmatrix} = \begin{bmatrix} A_f & A_f & A_f & A_f \\ -A_f & 0 & -A_f & 0 \\ 0 & -A_f & 0 & -A_f \\ M_c & M_c & M_c & M_c \end{bmatrix} \begin{bmatrix} \Omega_1^2 \\ \Omega_2^2 \\ \Omega_3^2 \\ \Omega_4^2 \end{bmatrix} \tag{2}$$

where T_1, T_2, T_3, and T_4 are the altitude, roll, pitch, and yaw control torques respectively, and A_f and M_c are the aerodynamic force and moment coefficients, respectively.

Lemma 1 ([35]). *If there exists a continuous positive definite function, V, satisfying $\dot{V} \leq -\bar{a}V^m + \bar{b}$, such that $\bar{a} > 0$, $\bar{b} > 0$, $0 < m \leq 1$ are real numbers, then the equilibrium point is semi-globally finite time stable.*

Lemma 2 ([59]). *RBFNN are widely used as function approximators in control system design due to their approximating capabilities. Consider the smooth function $N(Z) : \mathcal{R}^n \longrightarrow \mathcal{R}$, its RBFNN approximation can be expressed as*

$$N(Z) = W^T \xi(Z) + \vartheta$$

where $Z \in \mathcal{R}^N$ *is the RBFNN input vector, N is the dimension of Z,* $W = [w_1, w_2, \ldots w_m]^T$ *is the RBFNN weight vector,* $m > 1$ *is the number of RBFNN nodes,* $\xi = [\xi_1, \xi_2, \ldots, \xi_m]^T$ *is the Gaussian function given as*

$$\xi_i(Z) = exp\left[\frac{-(Z-\varsigma_i)^T(Z-\varsigma_i)}{2c_i^2}\right]$$

where $\varsigma_i = [\varsigma_{i1}, \varsigma_{i2}, \ldots, \varsigma_{im}]$ *is the center of the receptive field, and* c_i *is the center of the Gaussian function. If there exists* $\vartheta^* > 0$*, then* $\|\vartheta\| \leq \vartheta^*$ *must be satisfied.*

3. Quadrotor Control Design

This section presents a new control method for solving the trajectory tracking problem of a quadrotor. The quadrotor control system is divided into attitude and position control systems. The underactuation problem is solved by modifying the position subsystem. The objective is to design a compound controller, ANNBC-ANNBIFTSMC, to track the desired states, x_{1d} x_{3d} x_{5d}, x_{7d} x_{9d} x_{11d}. The block diagram of the proposed strategy is demonstrated in Figure 1.

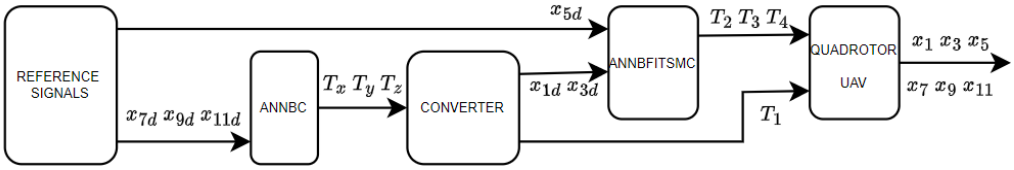

Figure 1. Control scheme of the quadrotor.

3.1. Position Control

In this section, the ANNBC is developed for the position subsystem of the quadrotor. The position subsystem can be written as

$$\begin{cases} \dot{x}_7 = x_8 \\ \dot{x}_8 = a_9 x_8 + T_x + \delta_{x_7} \\ \dot{x}_9 = x_{10} \\ \dot{x}_{10} = a_{10} x_{10} + T_y + \delta_{x_9} \\ \dot{x}_{11} = x_{12} \\ \dot{x}_{12} = a_{11} x_{12} + T_z + \delta_{x_{11}} \end{cases} \tag{3}$$

where δ_{x_7}, ΔT_x, δ_{x_9}, and $\delta_{x_{11}}$ are disturbances due to the environmental conditions and dynamic uncertainties.

$$\begin{cases} T_x = (C_{x_2} C_{x_5} S_{x_3} + S_{x_2} S_{x_5}) \frac{T_1}{m} \\ T_y = (C_{x_2} S_{x_3} S_{x_5} + C_{x_5} S_{x_2}) \frac{T_1}{m} \\ T_z = -g + (C_{x_2} C_{x_3}) \frac{T_1}{m} \end{cases} \tag{4}$$

To address the altitude tracking, the error variable is defined as $z_{11} = x_{11} - x_{11d}$. The derivative of z_{11} is

$$\dot{z}_{11} = \dot{x}_{11} - \dot{x}_{11d} = x_{12} - \dot{x}_{11d}. \tag{5}$$

Inserting $x_{12} = z_{12} + x_{12d}$ into (5) yields

$$\dot{z}_{11} = z_{12} + x_{12d} - \dot{x}_{11d}. \tag{6}$$

Consider a Lyapunov function as follows:

$$V_{11} = \frac{1}{2} z_{11}^2 \tag{7}$$

The derivative of V_{11} yields

$$\dot{V}_{11} = z_{11}\dot{z}_{11} = z_{11}z_{12} + z_{11}(x_{12d} - \dot{x}_{11d}). \tag{8}$$

Let the virtual control input be

$$x_{12d} = -M_{11}z_{11} + \dot{x}_{11d} \tag{9}$$

where $M_{11} > 0$ is a constant. Using (9), (8) becomes

$$\dot{V}_{11} = -M_{11}z_{11}^2 + z_{11}z_{12}. \tag{10}$$

The error between x_{12} and x_{12d} is

$$z_{12} = x_{12} - x_{12d}. \tag{11}$$

The time derivative of (11) gives

$$\dot{z}_{12} = \mathrm{a}_{11}x_{12} + T_z + \delta_{x_{11}} - \dot{x}_{12d}. \tag{12}$$

Note that $\dot{x}_{12d}$ is the derivative of the virtual input (9). Let $f_{11} = \mathrm{a}_{11}x_{12} - \dot{x}_{12d}$, which can be approximated by RBFNN as

$$f_{11} = W_{11}^T\xi_{11}(Z) + \vartheta_{11}. \tag{13}$$

Then, the adaptive altitude stabilizing controller can be designed as

$$T_z = -z_{11} - \hat{M}_{12}z_{12} - \hat{W}_{11}^T\xi_{11}(Z) - \hat{\delta}_{x_{11}}tanh\left(\frac{z_{11}}{\eta_{11}}\right). \tag{14}$$

The controller (14) is updated by

$$\begin{cases} \dot{\hat{M}}_{12} = \gamma_{12}[z_{12}^2 - \mu\hat{M}_{12}] \\ \dot{\hat{W}}_{11} = \gamma_{11}[z_{12}\xi_{12}(Z) - \mu\hat{W}_{11}] \\ \dot{\hat{\delta}}_{x11} = \pi_{11}\left(z_{12}tanh\left(\frac{z_{12}}{\eta_{11}}\right) - \mu\hat{\delta}_{x_{11}}\right) \end{cases} \tag{15}$$

where $\pi_{11} > 0$, $\gamma_{11} > 0$, $\gamma_{12} > 0$ are constants, and $\mu > 0$ is a small constant.

Theorem 1. *For the closed-loop system comprising the position subsystem* (3)*, control law* (14)*, and update law* (15)*, the error signals are semi-globally finite time stable.*

Proof. Consider a candidate Lyapunov function as

$$V_{12} = \frac{1}{2}z_{11}^2 + \frac{1}{2}z_{12}^2 + \frac{1}{2\gamma_{12}}\tilde{M}_{12}^2 + \frac{1}{2\gamma_{11}}\tilde{W}_{11}^2 + \frac{1}{2\pi_{11}}\tilde{\delta}_{x11}^2. \tag{16}$$

Differentiating V_{12} with respect to time gives

$$\begin{aligned} \dot{V}_{12} = {} & -M_{11}z_{11}^2 + z_{12}[z_{11} + W_{11}^T\xi_{11}(Z) + \vartheta + \delta_{x11} + T_z] \\ & + \frac{1}{\gamma_{12}}\tilde{M}_{12}\dot{\tilde{M}}_{12} + \frac{1}{\gamma_{11}}\tilde{W}_{11}\dot{\tilde{W}}_{11} + \frac{1}{\pi_{11}}\tilde{\delta}_{x11}\dot{\tilde{\delta}}_{x11} \end{aligned} \tag{17}$$

$$\dot{V}_{12} = -M_{11}z_{11}^2 + z_{12}\Bigg[W_{11}^T\xi_{11}(Z) + \vartheta - \hat{W}_{11}^T\xi_{11}(Z) - \hat{M}_{12}z_{12} + \delta_{x11} - \hat{\delta}_{x_{11}}tanh\left(\frac{z_{11}}{\eta_{11}}\right)\Bigg] - \frac{1}{\gamma_{12}}\tilde{M}_{12}\dot{\hat{M}}_{12} - \frac{1}{\gamma_{11}}\tilde{W}_{11}\dot{\hat{W}}_{11} - \frac{1}{\pi_{12}}\tilde{\delta}_{x_{11}}\dot{\hat{\delta}}_{x_{11}}. \tag{18}$$

Considering that $\hat{M}_{12} = M_{12} - \tilde{M}_{12}$, and adding $\delta_{x_{11}}tanh\left(\frac{z_{11}}{\eta_{11}}\right) - \delta_{x_{11}}tanh\left(\frac{z_{11}}{\eta_{11}}\right)$ to (18) we get:

$$\dot{V}_{12} = -M_{11}z_{11}^2 - M_{12}z_{12}^2 + \tilde{W}_{11}^T[z_{12}\xi_{11}(Z) - \frac{\dot{\hat{W}}_{11}}{\gamma_{11}}] + \tilde{M}_{12}[z_{12}^2 - \frac{\dot{\hat{M}}_{12}}{\gamma_{12}}] + \tilde{\delta}_{x11}[z_{12}tanh\left(\frac{z_{12}}{\eta_{11}}\right) - \frac{\dot{\hat{\delta}}_{x11}}{\pi_{11}}] + \delta_{x11}\left[z_{12} - z_{12}tanh\left(\frac{z_{12}}{\eta_{11}}\right)\right] + z_{12}\vartheta_{11}. \tag{19}$$

Substituting the adaptive laws (15) into (19) yields:

$$\dot{V}_{12} \leq -M_{11}z_{11}^2 - M_{12}z_{12}^2 + \mu\tilde{W}_{11}^T\hat{W}_{11} + \mu\tilde{M}_{12}\hat{M}_{12} + \mu\tilde{\delta}_{x11}\hat{\delta}_{x11} + \delta_{x11}\left[|z_{12}| - z_{12}tanh\left(\frac{z_{12}}{\eta_{11}}\right)\right] + z_{12}\vartheta_{11}. \tag{20}$$

Using Young's inequalities

$$\begin{cases} \tilde{M}_{11}\hat{M}_{11} = (M_{11} - \tilde{M}_{11})\tilde{M}_{11} \leq \frac{M_{11}^2}{2} - \frac{\tilde{M}_{11}^2}{2}; \\ \tilde{W}_{12}\hat{W}_{12} = (W_{12} - \tilde{W}_{12})\tilde{W}_{12} \leq \frac{W_{12}^2}{2} - \frac{\tilde{W}_{12}^2}{2}; \\ \tilde{\delta}_{x11}\hat{\delta}_{x11} \leq \frac{\delta_{x1}^2}{2} - \frac{\tilde{\delta}_{x11}^2}{2}; \\ z_{12}\vartheta_{11} \leq \frac{z_{12}^2}{2} + \frac{\vartheta_{11}^2}{2} \end{cases}$$

and the the identity $z_{12}tanh\left(\frac{z_{12}}{\eta_{12}}\right) - |z_{12}| \leq 0.2785\eta_{12}$, we have:

$$\dot{V}_{12} \leq -M_{11}z_{11}^2 - \left(M_{12} - \frac{1}{2}\right)z_{12}^2 - \mu\frac{\tilde{M}_{12}^2}{2} - \mu\frac{\tilde{W}_{11}^2}{2} - \mu\frac{\tilde{\delta}_{x11}^2}{2} + \mu\frac{M_{12}^2}{2} + \mu\frac{W_{11}^2}{2} + \frac{\vartheta_{11}^2}{2} + \frac{\delta_{x1}^2}{2} + \delta_{x11}\,.\,0.2785\eta_{12}. \tag{21}$$

Letting $\bar{a}_{12} = min\{2M_{11},\ 2\left(M_{12} - \frac{1}{2}\right),\ \mu\gamma_{12},\ \mu\gamma_{11},\ \mu\pi_{11}\}$, $\bar{b}_{12} = \mu\frac{M_{12}^2}{2} + \mu\frac{W_{11}^2}{2} + \frac{\vartheta_{11}^2}{2} + \frac{\delta_{x1}^2}{2} + \delta_{x11}\,.\,0.2785\eta_{12}$, one can get:

$$\dot{V}_{12} \leq -\bar{a}_{12}V_{12} + \bar{b}_{12}. \tag{22}$$

□

Therefore, considering Lemma 1, the closed loop signals are semi-globally finite time stable. In the same way as the altitude (x_{11}) control design, the control inputs for the positions x_7 and x_9 are derived as follows:

$$\begin{cases} T_x = -z_7 - \hat{M}_9 z_8 - \hat{W}_7 \xi_7(Z) - \hat{\delta}_{x_7} tanh\left(\frac{z_8}{\eta_7}\right) \\ T_y = -z_9 - \hat{M}_{10} z_{10} - \hat{W}_9 \xi_9(Z) - \hat{\delta}_{x_9} tanh\left(\frac{z_{10}}{\eta_9}\right). \end{cases} \tag{23}$$

The adaptation rules are given by

$$\begin{cases} \dot{\hat{M}}_8 = \gamma_8[z_8^2 - \mu \hat{M}_8] \\ \dot{\hat{W}}_7 = \gamma_7[z_8 \xi_7(Z) - \mu \hat{W}_7] \end{cases} \tag{24}$$

$$\begin{cases} \dot{\hat{M}}_{10} = \gamma_{10}[z_{10}^2 - \mu \hat{M}_{10}] \\ \dot{\hat{W}}_9 = \gamma_9[z_{10} \xi_9(Z) - \mu \hat{W}_9] \end{cases} \tag{25}$$

$$\begin{cases} \dot{\hat{\delta}}_{x7} = \pi_7\left(z_8 tanh\left(\frac{z_8}{\eta_7}\right) - \mu \hat{\delta}_{x_7}\right) \\ \dot{\hat{\delta}}_{x9} = \pi_9\left(z_{10} tanh\left(\frac{z_{10}}{\eta_9}\right) - \mu \hat{\delta}_{x_9}\right) \end{cases} \tag{26}$$

where $\gamma_i > 0$, $(i = 7, 8, 9, 10)$, $\pi_i > 0$, $(i = 7, 9)$, $\eta_i > 0$, $(i = 7, 9)$ are constants, and $\mu > 0$ is a small constant. The total thrust force is thus

$$T_1 = m\sqrt{T_x^2 + T_y^2 + (T_z + g)^2}. \tag{27}$$

The desired roll and pitch angles are computed as

$$\begin{cases} x_{1d} = arctan\left(C_{x_{3d}}\left(\frac{S_{x_{5d}} T_x - C_{x_{5d}} T_Y}{T_z + g}\right)\right) \\ x_{3d} = arctan\left(\frac{C_{x_{5d}} T_x + C_{x_{5d}} T_Y}{T_z + g}\right). \end{cases} \tag{28}$$

3.2. Attitude Control

In this section, the ANNBIFTSMC is developed for the attitude subsystem. The attitude subsystem can be written as

$$\begin{cases} \dot{x}_1 = x_2 \\ \dot{x}_2 = \pi_1^T \theta_1 + g_1 T_2 + d_1 \\ \dot{x}_3 = x_4 \\ \dot{x}_4 = \pi_2^T \theta_2 + g_2 T_3 + d_2 \\ \dot{x}_5 = x_6 \\ \dot{x}_6 = \pi_3^T \theta_3 + g_3 T_4 + d_3 \end{cases} \tag{29}$$

where $d_i = \Delta_i(\pi_i^T \theta_i + g_i T_{i+1}) + \delta_i$ $(i = 1, 2, 3)$ denote the lumped external disturbances and uncertainties,

$$\begin{aligned} &\pi_1 = \begin{bmatrix} a_2 & a_2 & a_3 \end{bmatrix}^T, \pi_2 = \begin{bmatrix} a_4 & a_5 & a_6 \end{bmatrix}^T, \\ &\pi_3 = \begin{bmatrix} a_7 & a_8 \end{bmatrix}^T, \theta_1 = \begin{bmatrix} x_4 x_6 & x_4 & x_2^2 \end{bmatrix}^T, \\ &\theta_2 = \begin{bmatrix} x_2 x_6 & x_2 & x_4^2 \end{bmatrix}^T, \theta_3 = \begin{bmatrix} x_2 x_4 & x_6^2 \end{bmatrix}^T \end{aligned}$$

Assumption 1. *The disturbances satisfy $d_i \leq r_i$ $(i = 1, 2, 3)$, with r_i being the upper bound of the disturbances.*

The trajectory tracking error of the roll angle, x_1, along x_{1d} is

$$z_1 = x_1 - x_{1d} \tag{30}$$

$$\dot{z}_1 = \dot{x}_1 - \dot{x}_{1d} = x_2 - \dot{x}_{1d}. \tag{31}$$

Construct a positive Lyapunov function of the form

$$V_1 = \frac{1}{2}z_1^2 \tag{32}$$

$$\dot{V}_1 = z_1\dot{z}_1 = z_1(x_2 - \dot{x}_{1d}). \tag{33}$$

The fictitious input that stabilizes x_1 is designed as

$$x_2 = S_1 - M_1 z_1 + \dot{x}_{1d} \tag{34}$$

where S_1 is the IFTSM surface. Inserting (34) into (33) gives

$$\dot{V}_1 = -M_1 z_1^2 + z_1 S_1. \tag{35}$$

The IFSMC surface is given by

$$S_1 = \dot{z}_1 + \Lambda_1 z_1 + \beta_1 \int_0^t (z_1 + \tau_1 z_1^{p/q})dt \tag{36}$$

where $\Lambda_1 > 0$, $\beta_1 > 0$, $\tau_1 > 0$ and $0 < p < q$ are design parameters. The derivative of S_1 with respect to time gives

$$\dot{S}_1 = \ddot{z}_1 + \Lambda_1\dot{z}_1 + \beta_1(z_1 + \tau_1 z_1^{p/q}) = f_1 + g_1 T_2 \tag{37}$$

where $f_1 = \pi_1^T\theta_1 + d_1 - \ddot{x}_{1d} + \Lambda_1\dot{z}_1 + \beta_1(z_1 + \tau_1 z_1^{p/q})$. Using RBFNN, f_1 can be approximated as

$$f_1 = W_1^T\xi_1(Z) + \vartheta_1. \tag{38}$$

The overall roll angle controller is calculated as

$$\begin{cases} T_2 = T_{2eq} + T_{2r} \\ T_{2eq} = g_1^{-1}[-z_1 - \hat{W}_1\xi_1(Z)] \\ T_{2r} = g_1^{-1}[-\hat{r}_1|S_1|^{p/q}sign(S_1) - \hat{K}_1 S_1] \end{cases} \tag{39}$$

where T_{2eq} and T_{2r} stand for the equivalent and the terminal reaching laws, respectively, and $\hat{r}_1$, $\hat{K}_1$, and $\hat{W}_1$ are the estimates of r_1, K_1, and W_1, respectively. The updating rules are designed as

$$\begin{cases} \dot{\hat{W}}_1 = \sigma_1[S_1\xi_1(Z) - \mu\hat{W}_1] \\ \dot{\hat{r}}_1 = \rho_1[|S_1|^{(1+p/q)} - \mu\hat{r}_1] \\ \dot{\hat{K}}_1 = \gamma_1[S_1^2 - \mu\hat{K}_1] \end{cases} \tag{40}$$

where $\gamma_1 > 0$ and $\rho_1 > 0$ are design parameters, and $\mu > 0$ is a small constant.

Theorem 2. *For the attitude subsystem* (29) *and the IFTSMC surface* (36)*, if the adaptive robust control inputs are established as* (39) *and updated by* (40)*, then all the error variables in the closed loop system are ultimately bounded.*

Proof. The Lyapunov function for estimating the parameters is constructed as

$$V_2 = \frac{z_1^2}{2} + \frac{S_1^2}{2} + \frac{\tilde{r}_1^2}{2\rho_1} + \frac{\tilde{K}_2^2}{2\gamma_1} + \frac{\tilde{W}_1^2}{2\sigma_1} \tag{41}$$

where $\tilde{r}_1 = r_1 - \hat{r}_1$ and $\tilde{K}_1 = K_1 - \hat{K}_1$ are estimation errors. The time derivative of the Lyapunov function (41) is

$$\begin{aligned}\dot{V}_2 &= z_1\dot{z}_1 + S_1\dot{S}_1 + \frac{\tilde{r}_1}{\rho_1}\dot{\tilde{r}}_1 + \frac{\tilde{K}_1}{\gamma_1}\dot{\tilde{K}}_1 + \frac{\tilde{W}_1}{\sigma_1}\dot{\tilde{W}}_1 \\ &= -M_1 z_1^2 + S_1\left[z_1 + W_1\xi_1(Z) + \vartheta_1 + g_1 T_2\right] \\ &- \frac{\tilde{r}_1}{\rho_1}\dot{\hat{r}}_1 - \frac{\tilde{K}_1}{\gamma_1}\dot{\hat{K}}_1 - \frac{\tilde{W}_1}{\sigma_1}\dot{\hat{W}}_1. \end{aligned} \tag{42}$$

Combining (39) and (42), we get

$$\begin{aligned}\dot{V}_2 &= -M_1 z_1^2 + S_1[\tilde{W}_1\xi_1(Z) + \vartheta_1 \\ &- \hat{r}_1|S_1|^{p/q}sign(S_1) - \hat{K}_1 S_1] \\ &- \frac{\dot{\hat{r}}_1}{\rho_1}\tilde{r}_1 - \frac{\dot{\hat{K}}_1}{\gamma_1}\tilde{K}_1 - \frac{\dot{\hat{W}}_1}{\sigma_1}\tilde{W}_1. \end{aligned} \tag{43}$$

Equation (43) can be rewritten as

$$\begin{aligned}\dot{V}_2 &\le -M_1 z_1^2 - K_1 S_1^2 + (\vartheta_1 - r_1|S_1|^{p/q})|S_1| \\ &+ \tilde{r}_1\left[|S_1|^{(1+p/q)} - \frac{\dot{\hat{r}}_1}{\rho_1}\right] \\ &+ \tilde{K}_1\left[S_1^2 - \frac{\dot{\hat{K}}_1}{\gamma_1}\right] + \tilde{W}_1\left[S_1\xi_1(Z) - \frac{\dot{\hat{W}}_1}{\sigma_1}\right]. \end{aligned} \tag{44}$$

By substituting (40) into (44), one has

$$\dot{V}_2 = -M_1 z_1^2 - K_1 S_1^2 - \bar{r}_1|S_1| + \mu\tilde{r}_1\hat{r}_1 + \mu\tilde{K}_1\hat{K}_1 + \mu\tilde{W}_1\hat{W}_1 \tag{45}$$

where $\bar{r}_1 = (r_1|S_1|^{p/q} - \vartheta_1)$ Using the following Young's inequalities,

$$\begin{cases} \tilde{W}_1\hat{W}_1 \le \frac{W_1^2}{2} - \frac{\tilde{W}_1^2}{2} \\ \tilde{K}_1\hat{K}_1 \le \frac{K_1^2}{2} - \frac{\tilde{K}_1^2}{2} \\ \tilde{r}_1\hat{r}_1 \le \frac{r_1^2}{2} - \frac{\tilde{r}_1^2}{2};\ \bar{r}_1|S_1| \le \frac{\bar{r}_1^2}{2} + \frac{|S_1|^2}{2} \end{cases}$$

we have

$$\begin{aligned}\dot{V}_2 &\le -M_1 z_1^2 - K_1 S_1^2 - \frac{|S_1|^2}{2} - \mu\frac{\tilde{r}_1^2}{2} - \mu\frac{\tilde{K}_1^2}{2} + \mu\frac{K_1^2}{2} \\ &+ \mu\frac{r_1^2}{2} - \frac{\bar{r}_1^2}{2} \\ &\le \bar{a}_1 V_2 + \bar{b}_1 \end{aligned} \tag{46}$$

where $\bar{a}_1 = min(2M_1, 2(K_1 + \frac{1}{2}), \mu, \mu)$, $\bar{b}_1 = \mu\frac{K_1^2}{2} + \mu\frac{r_1^2}{2} - \frac{\bar{r}_1^2}{2}$. Therefore, based on Lemma 1, the closed loop error signals are bounded. □

Following the same approach as the roll angle control design, the pitch angle (x_3) and the yaw angle (x_5) controllers are calculated as

$$T_3 = g_2^{-1}\left[-z_2 - \hat{W}_2^T\xi_2(Z) - \hat{r}_2|S_2|^{p/q}sign(S_2) - \hat{K}_2 S_2\right] \tag{47}$$

$$T_4 = g_3^{-1}\left[-z_3 - \hat{W}_3^T\xi_3(Z) - \hat{r}_3|S_3|^{p/q}sign(S_3) - \hat{K}_3 S_3\right]. \tag{48}$$

The updating rules are specified as

$$\begin{cases} \dot{\hat{W}}_2 = \sigma_2[S_2\xi_2(Z) - \mu\hat{W}_2] \\ \dot{\hat{r}}_2 = \rho_2[|S_2|^{(1+p/q)} - \mu\hat{r}_2] \\ \dot{\hat{K}}_2 = \gamma_2[S_2^2 - \mu\hat{K}_2] \end{cases} \tag{49}$$

$$\begin{cases} \dot{\hat{W}}_3 = \sigma_3[S_3\xi_3(Z) - \mu\hat{W}_3] \\ \dot{\hat{r}}_3 = \rho_3[|S_3|^{(1+p/q)} - \mu\hat{r}_3] \\ \dot{\hat{K}}_3 = \gamma_3[S_3^2 - \mu\hat{K}_3] \end{cases} \tag{50}$$

where $\gamma_i > 0$, $\rho_i > 0$, and $\sigma_i > 0$ $(i = 2, 3)$ are constants, and $\mu > 0$ is a small constant.

4. Simulation Results and Discussion

In this section, numerical simulations have been carried out on a quadrotor to demonstrate the satisfactory performance of the proposed hybrid control technique. The parameters of the quadrotor are the same as in [31]. The initial values of the quadrotor states for the simulations are $[0.01\ 0.01\ 0.01]m$ and $[0.01\ 0.01\ 0.01]rad$, and the initial values of the adaptive rules are set as 0.01 each. The reference signals for the quadrotor states are chosen as

$$x_d = \begin{cases} 0.8 & 0 \le t \le 10 \\ 0.6 & 10 < t \le 15 \\ 0.3 & 15 < t \le 20 \\ 0.8 & 20 < t \le 35 \end{cases} \; ; \; y_d = \begin{cases} 0.8 & 0 \le t \le 5 \\ 1.2 & 5 < t \le 15 \\ 0.6 & 15 < t \le 35 \end{cases}$$

$$z_d = \begin{cases} 0.7 & 0 \le t \le 10 \\ 0.4 & 10 < t \le 20 \\ & 20 < t \le 35 \end{cases} \; ; \; \psi_d = \begin{cases} & 0 \le t \le 15 \\ 0.2 & 15 < t \le 35 \end{cases}$$

We assumed a parametric variation of 40%, and the time-varying external disturbances are given by

$$\begin{bmatrix} \delta_{x_1} \\ \delta_{x_3} \\ \delta_{x_5} \end{bmatrix} = \begin{bmatrix} 0.2cos(2t) \\ 0.2sin(0.7t) \\ 0.2sin(t) \end{bmatrix}; \; \begin{bmatrix} \delta_{x_7} \\ \delta_{x_9} \\ \delta_{x_{11}} \end{bmatrix} = \begin{bmatrix} 0.2sin(2t) \\ 2cos(0.2t) \\ 0.2sin(0.8t) \end{bmatrix}$$

The gains of the controllers are given in Table 1.

In order to validate the superior performance of the proposed hybrid ANNBC-ANNBIFTSMC, comparisons with existing hierarchical controllers developed in [23,31] are provided. In [23], integral sliding mode control (ISMC) and backstepping sliding mode control (BSMC) were developed for the position and attitude subsystems of the quadrotor, respectively. In [31], neuro-adaptive sliding mode controller (NNSMC) and robust integral of the signum error (RISE) were designed for the position and attitude subsystems of the quadrotor, respectively. The trajectory tracking results of the quadrotor position depicted in Figure 2, along with the tracking errors in Figure 3 show that the three control strategies can accomplish a stable flight in general. However, the ISMC provides the lowest tracking performances compared to both ANNBC and NNSMC. Due to the approximation property of the RBFNN to estimate the time-varying disturbances, the NNSMC shows an improved performance compared to the ISMC. The proposed ANNBC gives the most promising performance because of its ability to adjust its gains with abrupt change in the reference trajectories and to approximate and compensate the time-varying disturbances using the RBFNN. The gains of the ANNBC are presented in Figure 4.

Table 1. Control system parameters.

Controllers	Parameters	Values
ANNBC	M_7, M_9, M_{11}	10, 10, 10
	$\gamma_8, \gamma_{10}, \gamma_{12}$	12, 12, 12
	$\gamma_7, \gamma_9, \gamma_{11}$	0.2, 0.2, 0.2
	ς_i	$\begin{bmatrix} 0 & 0.2 & 0.4 & 0.6 & 0.8 \\ 0 & 0.2 & 0.4 & 0.6 & 0.8 \end{bmatrix}$
	$c_i,\ \mu$	0.4, 0.01
ANNBIFTSMC	$\Lambda_1, \Lambda_2, \Lambda_3$	5, 5, 1.5
	$\beta_1, \beta_2, \beta_3$	8, 8, 20
	τ_1, τ_2, τ_3	0.05, 0.05, 0.05
	$\gamma_1, \gamma_2, \gamma_3$	0.4, 0.4, 0.15
	ρ_1, ρ_2, ρ_3	0.3, 0.3, 0.3
	$\sigma_1, \sigma_2, \sigma_3$	0.2, 0.2, 0.2
	ς_i	$\begin{bmatrix} 0 & 0.2 & 0.4 & 0.6 & 0.8 \\ 0 & 0.2 & 0.4 & 0.6 & 0.8 \end{bmatrix}$
	$c_i,\ \mu$	0.4, 0.01

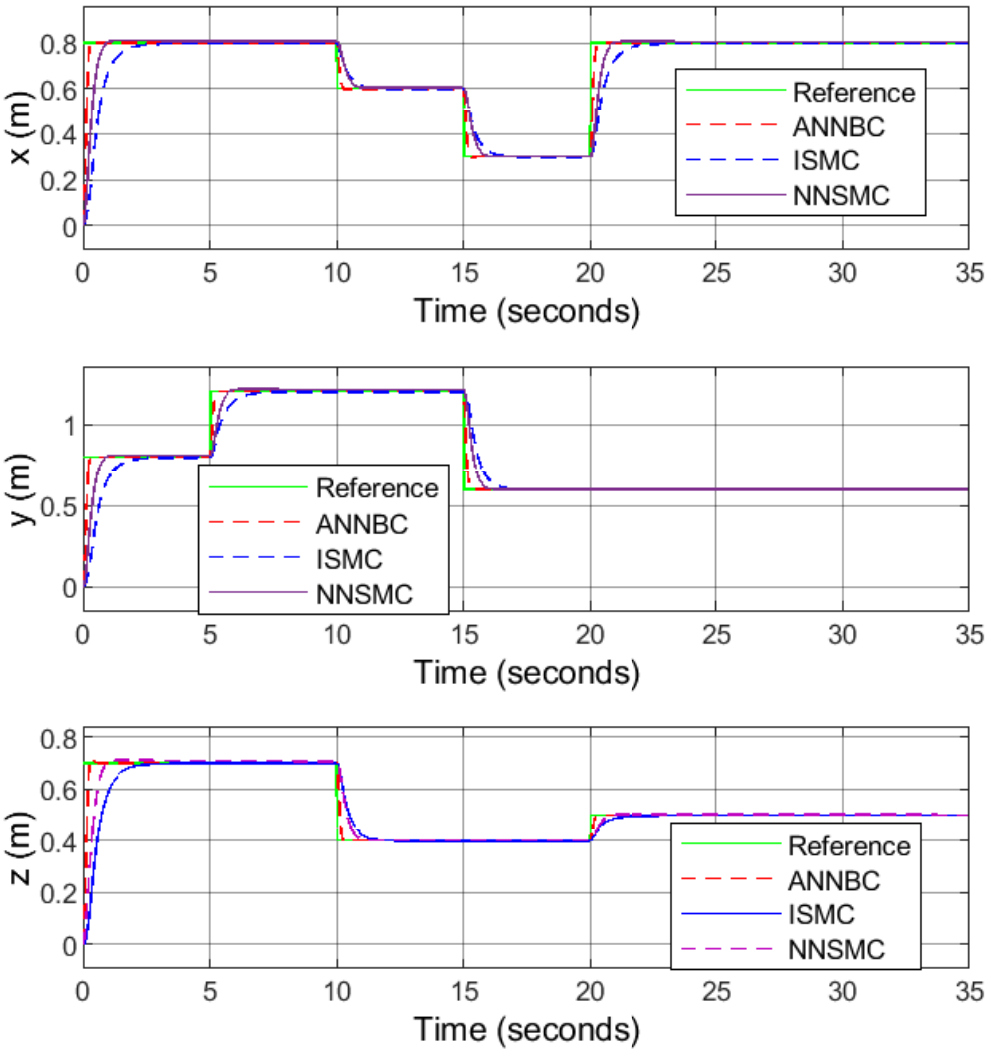

Figure 2. Position tracking results.

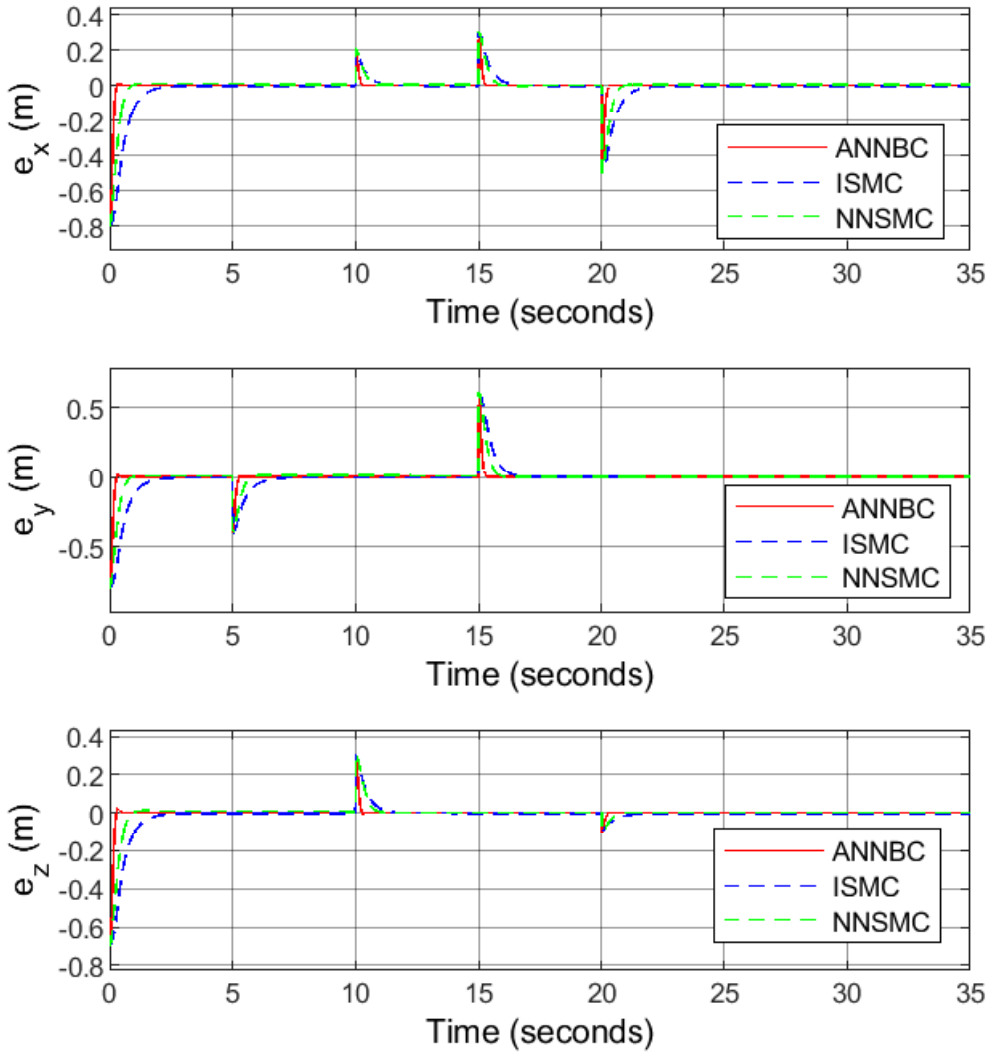

Figure 3. Position tracking error results.

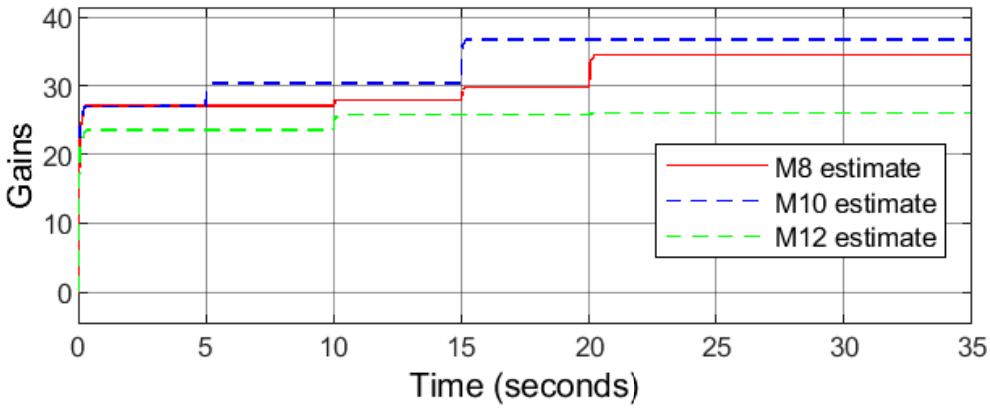

Figure 4. Estimates of M_8, M_{10}, and M_{12}.

The attitude responses are shown in Figure 5. It can be observed that the proposed ANNBIFTSMC provides more accurate tracking under the parametric uncertainties, time-varying disturbances, and sudden change in reference trajectories. Although both BSMC and RISE are robust to disturbances, the ANNBIFTSMC outperformed them because it combined the advantages of an integral error term to remove the steady state errors,

a nonlinear error term for fast convergence, a backstepping approach for guaranteed stability, and RBFNN for estimating disturbances. In addition, the tracking error responses of the yaw angle presented in Figure 6 further illustrate the convergence speed of the ANNBIFTSMC compared with the other controllers. The evolution of the gains of the fast terminal reaching laws are depicted in Figures 7 and 8. As shown in Figure 9, the control signals are free from chattering phenomena.

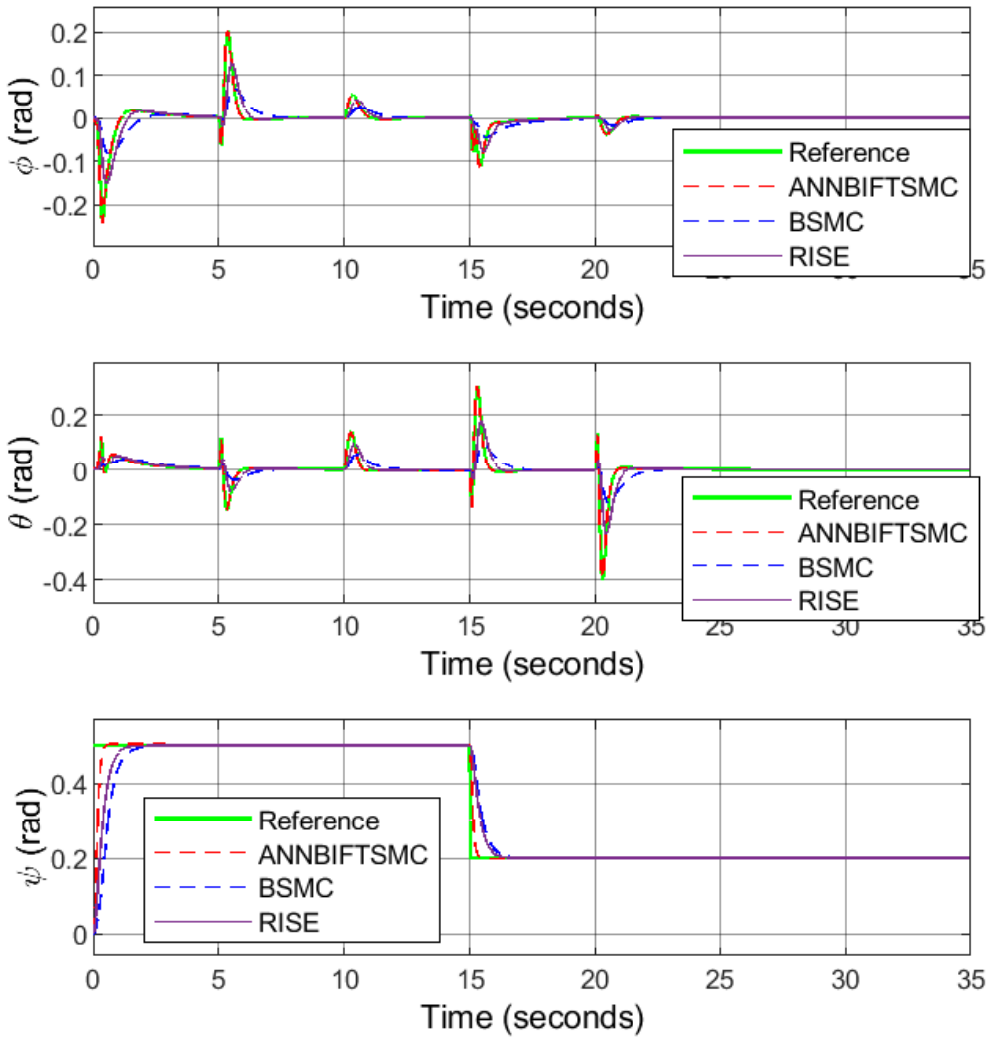

Figure 5. Attitude tracking results.

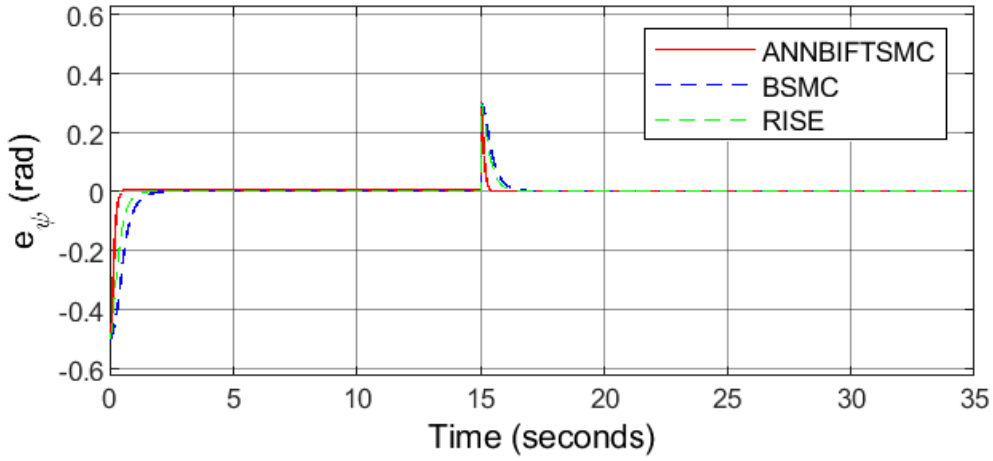

Figure 6. Attitude tracking error results.

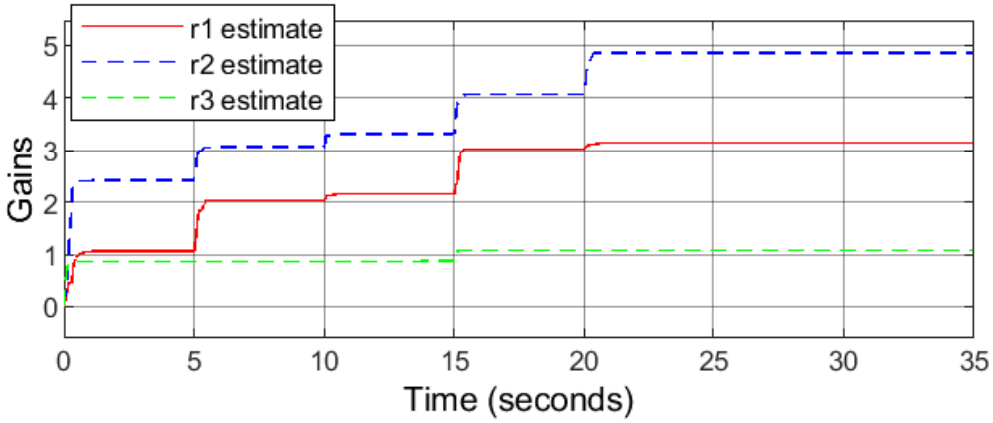

Figure 7. Estimates of r_1, r_2, and r_3.

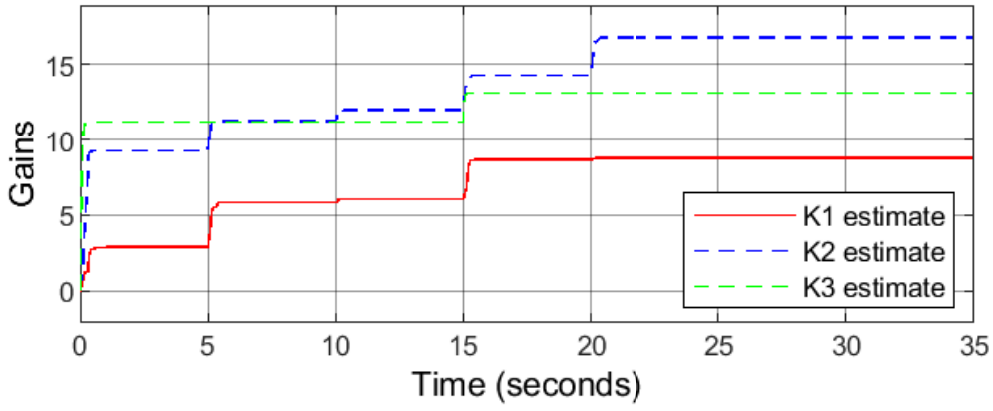

Figure 8. Estimates of K_1, K_2, and K_3.

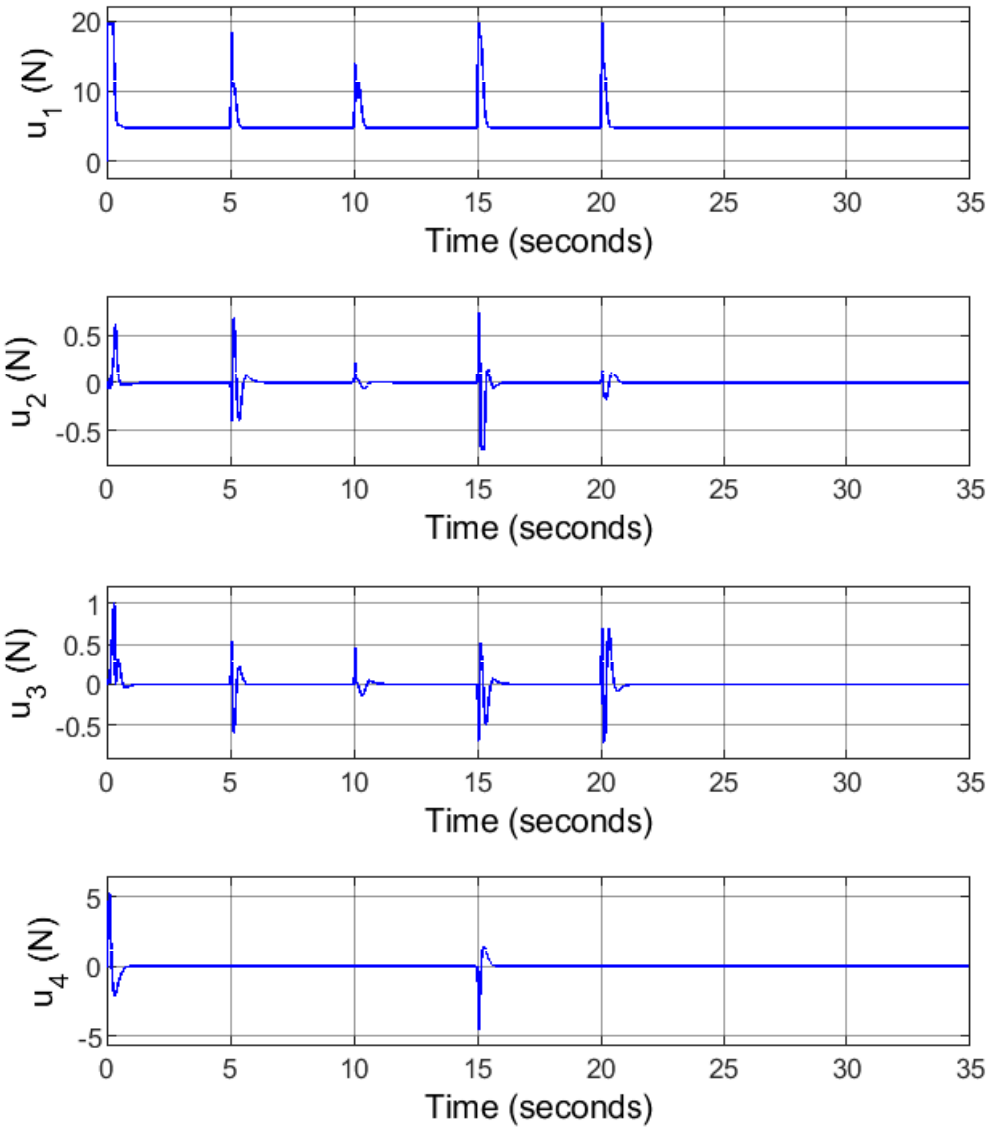

Figure 9. Quadrotor control inputs.

5. Conclusions

In this paper, the trajectory tracking control of a quadrotor with dynamic uncertainties and external disturbances was presented. The proposed hybrid control method consists of two components: attitude control and position control. The attitude control was designed to meet the requirements of fast response and robustness, and the position control was designed to achieve high tracking accuracy. First, the position subsystem was controlled using ANNBC. Then, an ANNBIFTSMC was designed to control the attitude subsystem. In essence, the RBFNN approximates and compensates for complex disturbances and model uncertainties. To avoid selecting improper gains, the proposed ANNBC-ANNBIFTSMC gains are updated online by adaptation rules. We eliminated the chattering phenomenon by using fast terminal reaching laws. Furthermore, the overall ANNBC-ANNBIFTSMC system was implemented to achieve an optimal balance between robustness and performance. Numerical simulation results indicate that the ANNBC-ANNBIFTSMC has the edge over some control schemes in terms of trajectory tracking accuracy and robustness to external disturbances.

Author Contributions: Methodology, M.M., W.M.H. and M.A.A.; Software, M.M.; Validation, W.M.H.; Investigation, W.M.H.; Writing—original draft, M.M.; Writing—review and editing, W.M.H. and M.A.A.; Supervision, M.A.A. All authors have read and agreed to the published version of the manuscript.

Funding: Interdisciplinary Research Center for Renewable Energy and Power Systems, King Fahd University of Petroleum and Minerals (KFUPM), Dhahran, Saudi Arabia, through the funded project INRE2103.

Data Availability Statement: Not applicable.

Acknowledgments: The authors acknowledge the support provided by Interdisciplinary Research Center for Renewable Energy and Power Systems, King Fahd University of Petroleum & Minerals (KFUPM), Dhahran, Saudi Arabia, through the funded project # INRE2103. Abido would like to acknowledge also KACARE Energy Research & Innovation Center, KFUPM.

Conflicts of Interest: The authors declare no conflict of interest.

References

1. Rendón, M.; Martins, F.; Ganimi, L. A Visual Interface Tool for Development of Quadrotor Control Strategies. *J. Intell. Robot. Syst.* **2020**, *14*, 223–230. [CrossRef]
2. Saif, E.; Eminoğlu, İ. Modelling of quad-rotor dynamics and Hardware-in-the-Loop simulation. *J. Eng.* **2022**, *2022*, 937–950. [CrossRef]
3. Shao, S.; Chen, M.; Hou, J.; Zhao, Q. Event-Triggered-Based Discrete-Time Neural Control for a Quadrotor UAV Using Disturbance Observer. *IEEE/ASME Trans. Mechatron.* **2021**, *26*, 689–699. [CrossRef]
4. Tang, Z.; Cunha, R.; Cabecinhas, D.; Hamel, T.; Silvestre, C. Quadrotor going through a window and landing: An image-based visual servo control approach. *Control Eng. Pract.* **2021**, *112*, 104827. . [CrossRef]
5. Zamoum, Y.; Baiche, K.; Benkada, K.M.; Rahou, M.; Boushaki, R.; Kouzou, A. Control of the Lateral and Longitudinal Dynamics of UAV Quadcopter. In Proceedings of the 2022 19th International Multi-Conference on Systems, Signals & Devices (SSD), Setif, Algeria, 6–10 May 2022; pp. 595–600.
6. Tayebi, A.; McGilvray, S. Attitude stabilization of a VTOL quadrotor aircraft. *IEEE Trans. Control Syst. Technol.* **2006**, *14*, 562–571. [CrossRef]
7. Bouabdallah, S.; Noth, A.; Siegwart, R. PID vs. LQ control techniques applied to an indoor micro quadrotor. In Proceedings of the 2004 IEEE/RSJ International Conference on Intelligent Robots and Systems (IROS) (IEEE Cat. No.04CH37566), Sendai, Japan, 28 September–2 October 2004; Volume 3, pp. 2451–2456.
8. Hamanah, W.M.; Abido, M.A.; Alhems, L.M. Optimum Sizing of Hybrid PV, Wind, Battery and Diesel System Using Lightning Search Algorithm. *Arab. J. Sci. Eng.* **2020**, *45*, 1871–1883. [CrossRef]
9. Pounds, P.E.I.; Bersak, D.R.; Dollar, A.M. Stability of small-scale UAV helicopters and quadrotors with added payload mass under PID control. *Auton. Robot.* **2012**, *33*, 129–142. [CrossRef]
10. Reyes-Valeria, E.; Enriquez-Caldera, R.; Camacho-Lara, S.; Guichard, J. LQR control for a quadrotor using unit quaternions: Modeling and simulation. In Proceedings of the CONIELECOMP 2013—23rd International Conference on Electronics, Communications and Computing, Puebla, Mexico, 11–13 March 2013; pp. 172–178.
11. Islam, M.; Okasha, M.; Idres, M.M. Trajectory tracking in quadrotor platform by using PD controller and LQR control approach. *IOP Conf. Ser. Mater. Sci. Eng.* **2017**, *260*, 012026. [CrossRef]
12. Xuan-Mung, N.; Hong, S.K. Improved altitude control algorithm for quadcopter unmanned aerial vehicles. *Appl. Sci.* **2019**, *9*, 2122. [CrossRef]
13. Liu, P.; Ye, R.; Shi, K.; Yan, B. Full Backstepping Control in Dynamic Systems With Air Disturbances Optimal Estimation of a Quadrotor. *IEEE Access* **2021**, *9*, 34206–34220. [CrossRef]
14. Moeini, A.; Lynch, A.F.; Zhao, Q. A backstepping disturbance observer control for multirotor UAVs: Theory and experiment. *Int. J. Control* **2021**, *95*, 2364–2378. [CrossRef]
15. Labbadi, M.; Boukal, Y.; Cherkaoui, M.; Djemai, M. Fractional-order global sliding mode controller for an uncertain quadrotor UAVs subjected to external disturbances. *J. Frankl. Inst.* **2021**, *358*, 4822–4847. . [CrossRef]
16. Ou, T.; Liu, Y. Adaptive Backstepping Tracking Control for Quadrotor Aerial Robots Subject to Uncertain Dynamics. In Proceedings of the 2019 American Control Conference (ACC), Philadelphia, PA, USA, 10–12 July 2019; pp. 1–6.
17. Guettal, L.; Chelihi, A.; Ajgou, R.; Touba, M.M. Robust tracking control for quadrotor with unknown nonlinear dynamics using adaptive neural network based fractional-order backstepping control. *J. Frankl. Inst.* **2022**, *359*, 7337–7364. [CrossRef]
18. Zhou, B.; Pan, J.; Gao, F.; Shen, S. RAPTOR: Robust and Perception-Aware Trajectory Replanning for Quadrotor Fast Flight. *IEEE Trans. Robot.* **2021**, *37*, 1992–2009. [CrossRef]
19. Huang, Y.; Zhu, M.; Sun, L.; Zheng, Z.; Jin, C. Adaptive backstepping control for autonomous shipboard landing of a quadrotor with input saturation. *Asian J. Control* **2021**, *23*, 1693–1706. [CrossRef]

20. Han, T.; Hu, Q.; Shin, H.S.; Tsourdos, A.; Xin, M. Sensor-based robust incremental three-dimensional guidance law with terminal angle constraint. *J. Guid. Control Dyn.* **2021**, *44*, 2016–2030. [CrossRef]
21. Baraean, A.; Hamanah, W.M.; Bawazir, A.; Baraean, S.; Abido, M.A. Optimal Nonlinear backstepping controller design of a Quadrotor-Slung load system using particle Swarm Optimization. *Alexandria Engineering Journal.* **2023**, *68*, 551–560. [CrossRef]
22. Han, T.; Shin, H.S.; Hu, Q.; Tsourdos, A.; Xin, M. Differentiator-Based Incremental Three-Dimensional Terminal Angle Guidance With Enhanced Robustness. *IEEE Trans. Aerosp. Electron. Syst.* **2022**, *58*, 4020–4032. [CrossRef]
23. Almakhles, D.J. Robust Backstepping Sliding Mode Control for a Quadrotor Trajectory Tracking Application. *IEEE Access* **2020**, *8*, 5515–5525. [CrossRef]
24. Wu, X.; Xiao, B.; Qu, Y. Modeling and sliding mode-based attitude tracking control of a quadrotor UAV with time-varying mass. *ISA Trans.* **2019**, *124*, 436–443. [CrossRef]
25. Muñoz, F.; González-Hernández, I.; Salazar, S.; Espinoza, E.S.; Lozano, R. Second order sliding mode controllers for altitude control of a quadrotor UAS: Real-time implementation in outdoor environments. *Neurocomputing* **2017**, *233*, 61–71. [CrossRef]
26. Alqaisi, W.; Ghommam, J.; Alazzam, A.; Saad, M.; Nerguizian, V. Three-loop uncertainties compensator and sliding mode quadrotor control. *Comput. Electr. Eng.* **2020**, *81*, 106507. [CrossRef]
27. Xiong, J.J.; Zhang, G.B. Global fast dynamic terminal sliding mode control for a quadrotor UAV. *ISA Trans.* **2017**, *66*, 233–240. [CrossRef] [PubMed]
28. Tripathi, V.K.; Kamath, A.K.; Behera, L.; Verma, N.K.; Nahavandi, S. An Adaptive Fast Terminal Sliding-Mode Controller with Power Rate Proportional Reaching Law for Quadrotor Position and Altitude Tracking. *IEEE Trans. Syst. Man Cybern. Syst.* **2021**, *52*, 3612–3625. [CrossRef]
29. Wang, Y.; Cao, K. Integral Terminal Sliding Mode-Based Flight Control for Quadrotor UAVs. In Proceedings of the 2019 Eleventh International Conference on Advanced Computational Intelligence (ICACI), Guilin, China, 7–9 June 2019; pp. 78–83.
30. Mechali, O.; Xu, L.; Huang, Y.; Shi, M.; Xie, X. Observer-based fixed-time continuous nonsingular terminal sliding mode control of quadrotor aircraft under uncertainties and disturbances for robust trajectory tracking: Theory and experiment. *Control Eng. Pract.* **2021**, *111*, 104806. [CrossRef]
31. Li, Z.; Ma, X.; Li, Y. Robust tracking control strategy for a quadrotor using RPD-SMC and RISE. *Neurocomputing* **2019**, *331*, 312–322. [CrossRef]
32. Xiong, J.; Guo, N.; Hong, Y.; Zheng, E. Improved Position and Attitude Tracking Control for a Quadrotor UAV. In Proceedings of the 2019 Chinese Automation Congress (CAC), Hangzhou, China, 22–24 November 2019; pp. 4197–4201.
33. Nian, X.; Chen, W.; Chu, X.; Xu, Z. Robust adaptive fault estimation and fault tolerant control for quadrotor attitude systems. *Int. J. Control* **2020**, *93*, 725–737. [CrossRef]
34. Ma, D.; Xia, Y.; Shen, G.; Jia, Z.; Li, T. Flatness-based adaptive sliding mode tracking control for a quadrotor with disturbances. *J. Frankl. Inst.* **2018**, *355*, 6300–6322. [CrossRef]
35. Mofid, O.; Mobayen, S. Adaptive sliding mode control for finite-time stability of quad-rotor UAVs with parametric uncertainties. *ISA Trans.* **2018**, *72*, 1–14. [CrossRef]
36. Lee, J.W.; Xuan-Mung, N.; Nguyen, N.P.; Hong, S.K. Adaptive altitude flight control of quadcopter under ground effect and time-varying load: Theory and experiments. *J. Vib. Control* **2023**, *29*, 571–581. [CrossRef]
37. He, Z.; Zhao, L.; Zhao, L. Robust chattering free backstepping/backstepping sliding mode control for quadrotor hovering. In Proceedings of the 2016 IEEE Information Technology, Networking, Electronic and Automation Control Conference, Chongqing, China, 20–22 May 2016; pp. 616–620.
38. Jia, Z.; Yu, J.; Mei, Y.; Chen, Y.; Shen, Y.; Ai, X. Integral backstepping sliding mode control for quadrotor helicopter under external uncertain disturbances. *Aerosp. Sci. Technol.* **2017**, *68*, 299–307. [CrossRef]
39. Labbadi, M.; Cherkaoui, M. Robust adaptive backstepping fast terminal sliding mode controller for uncertain quadrotor UAV. *Aerosp. Sci. Technol.* **2019**, *93*, 105306. [CrossRef]
40. Xuan-Mung, N.; Nguyen, N.P.; Nguyen, T.; Pham, D.B.; Vu, M.T.; Thanh, H.L.N.N.; Hong, S.K. Quadcopter precision landing on moving targets via disturbance observer-based controller and autonomous landing planner. *IEEE Access* **2022**, *10*, 83580–83590. [CrossRef]
41. Hernández-González, O.; Guerrero-Sánchez, M.E.; Farza, M.; Ménard, T.; M'Saad, M.; Lozano, R. High gain observer for a class of nonlinear systems with coupled structure and sampled output measurements: Application to a quadrotor. *Int. J. Syst. Sci.* **2019**, *50*, 1089–1105. [CrossRef]
42. Liu, K.; Wang, R.; Zheng, S.; Dong, S.; Sun, G. Fixed-time disturbance observer-based robust fault-tolerant tracking control for uncertain quadrotor UAV subject to input delay. *Nonlinear Dyn.* **2022**, *107*, 2363–2390. [CrossRef]
43. Li, B.; Zhang, H.; Niu, Y.; Ran, D.; Xiao, B. Finite-time disturbance observer-based trajectory tracking control for quadrotor unmanned aerial vehicle with obstacle avoidance. *Math. Methods Appl. Sci.* **2023**, *46*, 1096–1110. [CrossRef]
44. Chen, F.; Jiang, R.; Zhang, K.; Jiang, B.; Tao, G. Robust Backstepping Sliding-Mode Control and Observer-Based Fault Estimation for a Quadrotor UAV. *IEEE Trans. Ind. Electron.* **2016**, *63*, 5044–5056. [CrossRef]
45. Zhang, J.; Gu, D.; Deng, C.; Wen, B. Robust and Adaptive Backstepping Control for Hexacopter UAVs. *IEEE Access* **2019**, *7*, 163502–163514. [CrossRef]
46. Xuan Mung, N.; Nguyen, N.P.; Pham, D.B.; Dao, N.N.; Hong, S.K. Synthesized Landing Strategy for Quadcopter to Land Precisely on a Vertically Moving Apron. *Mathematics* **2022**, *10*, 1328. [CrossRef]

47. Li, J.; Liu, J.; Huangfu, S.; Cao, G.; Yu, D. Leader-follower formation of light-weight UAVs with novel active disturbance rejection control. *Appl. Math. Model.* **2023**, *117*, 577–591. [CrossRef]
48. Liu, X.; Gao, Q.; Ji, Y.; Song, Y.; Liu, J. Active Disturbance Rejection Control of Quadrotor UAV based on Whale Optimization Algorithm. In Proceedings of the 2022 IEEE International Conference on Mechatronics and Automation (ICMA), Guilin, China, 7–10 August 2022; pp. 351–356.
49. Park, S.; Han, S. Robust Backstepping Control Combined with Fractional-Order Tracking Differentiator and Fractional-Order Nonlinear Disturbance Observer for Unknown Quadrotor UAV Systems. *Appl. Sci.* **2022**, *12*, 11637. [CrossRef]
50. Wang, J.; Tian, Y.; Hua, L.; Shi, K.; Zhong, S.; Wen, S. New Results on Finite-Time Synchronization Control of Chaotic Memristor-Based Inertial Neural Networks with Time-Varying Delays. *Mathematics* **2023**, *11*, 684. [CrossRef]
51. Abdollahi, T.; Salehfard, S.; Xiong, C.; Ying, J. Simplified fuzzy-Padé controller for attitude control of quadrotor helicopters. *IET Control Theory Appl.* **2018**, *12*, 310–317. [CrossRef]
52. Barghandan, S.; Badamchizadeh, M.A.; Jahed-Motlagh, M.R. Improved adaptive fuzzy sliding mode controller for robust fault tolerant of a Quadrotor. *Int. J. Control Autom. Syst.* **2017**, *15*, 427–441. [CrossRef]
53. Liu, W.; Cheng, X.; Zhang, J. Command filter-based adaptive fuzzy integral backstepping control for quadrotor UAV with input saturation. *J. Frankl. Inst.* **2023**, *360*, 484–507. [CrossRef]
54. Ullah, S.; Khan, Q.; Mehmood, A.; Kirmani, S.A.M.; Mechali, O. Neuro-adaptive fast integral terminal sliding mode control design with variable gain robust exact differentiator for under-actuated quadcopter UAV. *ISA Trans.* **2022**, *120*, 293–304. [CrossRef]
55. Ullah, M.; Zhao, C.; Maqsood, H.; Nasir, A.; Humayun, M.; Hassan, M.U.; Alam, F. Adaptive Neural-Sliding Mode Control of a Quadrotor Vehicle with Uncertainties and Disturbances Compensation. In Proceedings of the 2022 2nd International Conference on Artificial Intelligence (ICAI), Islamabad, Pakistan, 30–31 March 2022; pp. 38–45.
56. Lin, X.; Wang, Y.; Liu, Y. Neural-network-based robust terminal sliding-mode control of quadrotor. *Asian J. Control* **2022**, *24*, 427–438. [CrossRef]
57. ul Amin, R.; Inayat, I.; Jun, L.A. Finite time position and heading tracking control of coaxial octorotor based on extended inverse multi-quadratic radial basis function network and external disturbance observer. *J. Frankl. Inst.* **2019**, *356*, 4240–4269. [CrossRef]
58. Shao, X.; Liu, N.; Wang, Z.; Zhang, W.; Yang, W. Neuroadaptive integral robust control of visual quadrotor for tracking a moving object. *Mech. Syst. Signal Process.* **2020**, *136*, 106513. [CrossRef]
59. Vafamand, N.; Arefi, M.M. Robust neural network-based backstepping landing control of quadrotor on moving platform with stochastic noise. *Int. J. Robust Nonlinear Control* **2022**, *32*, 2007–2026. [CrossRef]